

Development and verification of self-sensing structures printed in additive manufacturing: a preliminary study

Antonino Quattrocchi¹, Roberto Montanini¹

¹ Department of Engineering, University of Messina, C.da di Dio, 98166 Messina, Italy

ABSTRACT

Additive Manufacturing (AM) is used today to fabricate complex structures as well as to demonstrate innovative design concepts. This opens new horizons in the field of Structural Health Monitoring (SHM), allowing to correlate a high performing design with real-time detection and identification of the structural damage. Fiber optical sensors, such as Fiber Bragg Gratings (FBGs), are an effective option for this type of applications. The present work discusses the development of a demonstrative self-sensing structure, obtained by embedding a FBG sensor during the 3D stereolithographic (SLA) printing process. The paper reports the strategies developed in order to ensure a correct adhesion of the FBG sensor embedded into the structure and the experimental tests used for validating the structural response of the self-sensing specimen. The output signal of the FBG sensor was continuously recorded during the different stages of the creation phases: this allowed real-time monitoring of the whole AM process (i.e. printing, washing and curing stages). The obtained results showed that the self-sensing demonstrative structure was able to effectively monitor the thermo-mechanical behavior of the AM process and to guarantee the correct identification and measurement of the strain as the same structure was subjected to a controlled stress.

Section: RESEARCH PAPER

Keywords: Fiber Bragg grating sensor; stereolithography; embedded sensors; 3D printing monitoring; stress-strain measurements

Citation: Antonino Quattrocchi, Roberto Montanini, Development and verification of self-sensing structures printed in additive manufacturing: a preliminary study, Acta IMEKO, vol. 12, no. 2, article 25, June 2023, identifier: IMEKO-ACTA-12 (2023)-02-25

Section Editor: Alfredo Cigada, Politecnico di Milano, Italy, Andrea Scorza, Università Degli Studi Roma Tre, Italy

Received December 14, 2022; **In final form** February 27, 2023; **Published** June 2023

Copyright: This is an open-access article distributed under the terms of the Creative Commons Attribution 3.0 License, which permits unrestricted use, distribution, and reproduction in any medium, provided the original author and source are credited.

Funding: This work was supported by the Ministry of University and Research in Italy (MUR) under the Research Project of the National Operative Program (PON "Ricerca e Innovazione 2014 e 2020") "NAUSICA - Efficient ships through the use of innovative and low Carbon technological solutions".

Corresponding author: Antonino Quattrocchi, e-mail: antonino.quattrocchi@unime.it

1. INTRODUCTION

Technological innovation is increasingly oriented towards the development of systems that allow monitoring of the health state of structures (Structural Health Monitoring, SHM). In this way, structural damage can be early detected and identified by means of sensors integrated into the structure itself, which are therefore able to evaluate the degradation in real time [1]. Such sensors are preferred, compared to conventional transduction devices, because they are protected from atmospheric agents and can be placed more easily in critical points of the structure, also in areas that are difficult to reach from the outside [2]. On the other hand, their installation must be foreseen when the structure is designed or as retrofitting, since an easy intervention to restore the malfunctioning sensor is not possible [3].

Fiber optical sensors, specifically Fiber Bragg grating (FBG), are suitable for the production of smart structures [4]. They have

numerous advantages, such as low intrusiveness, immunity to electromagnetic interference, self-referentiality, absence of corrosion and the possibility of creating sensor networks with many measurement points. Instead, the main drawbacks concern the significant influence from the temperature, the limited opportunity of imparting a curvature to the fiber to avoid signal losses, the relatively high cost of both the sensors and the interrogation devices necessary for the measurement [5]-[7]. A FBG sensor can be installed onto different materials by applying ribbon tapes, glues or epoxy resins. However, these methods are time-consuming, require different molds or tools and induce variability in the measurement of the considered property [8]-[10]. Alternatively, in the case of composites and reinforced concretes, the integration of such sensors can be performed during the stratification of the structure [11], [12].

The rapid diffusion of Additive Manufacturing (AM) in a perspective of Industry 4.0 opens new possibilities in the field of SHM, enabling the design of complex and topologically

optimized structural elements [13], [14]. Nowadays several AM methods are available, among which the most popular are Fused Deposition Modeling (FDM), stereolithography (SLA) and Selective Laser Sintering (SLS). Although in all cases the objects are produced by sequential layer deposition of material, there are substantial differences in the stratification process [15], [16].

In this context, the use of a FBG sensor to ensure a self-sensing capability to a 3D printed structure assumes great relevance. Among the first researchers, Zobel et al. [17] demonstrated the possibility of incorporating some FBG sensors into a patch to estimate strain and temperature. Lima et al. [18] proposed a cantilever structure to evaluate displacement, temperature and acceleration. Lesiak et al. [19] verified this approach also to produce a measuring head implanted into a mechanical transmission element, while Zhang et al. [20] created a plantar pressure sensing platform.

A large part of the literature discusses the case of FDM-printed structures, where the incorporation process of the FBG sensors generally follows two different procedures. In the first one [21], the whole structure is printed and equipped with a small channel, where the FBG sensor is inserted and glued. Instead, in the second one, the structure is only partially realized, temporarily stopping the printing. Then the FBG sensor is placed directly onto the superficial layer [22], [23] or inside a small housing channel [24]. Finally, the stratification of the remaining layers goes to completed. In this way, the molding of the polymer filament is exploited to cover the FBG sensor and connect it to the structure. Currently few articles discuss the case of SLA, whereby pausing the process is more complex. In fact, the manufactured object is alternative immersed in and extracted from the liquid bath in order to create the single layer and to mix the printing material, respectively. Such printing material is generally a resin, characterized by a high viscosity at the liquid state. Consequently, the solidified layer always remains wet and this is the main cause of the difficulty of correctly placing the FBG sensor [25]. Recently Manzo et al. [26] have analytically and experimentally investigated two different applications, a reduced-scale frame structure and a pressurized cylindrical vessel, obtained by SLA. The authors have embedded the FBG sensor filling a thin channel with the printing material (resin). This has involved a considerable attention to avoid air bubbles and the need to cure the resin inserted into the channel.

The aim of this work is to discuss the development of a self-sensing structure with embedded FBG, using SLA. At first, two different procedures for the integration of the FBG sensor were discussed, highlighting their advantages and disadvantages. After

identifying the best configuration, the FBG sensor was exploited to monitor the whole AM process (i.e. printing, washing and curing stages) of the self-sensing structure, also making use of additional strategies to compensate for the effects of the temperature. Finally, the structural response of the realized self-sensing sample was evaluated by subjecting it to a controlled stress.

2. MATERIALS AND METHODS

2.1. Printing of the self-sensing structures

The representative test sample of the developed self-sensing structure was manufactured by an SLA printer (mod. Form 2, Formlabs), using a photopolymer resin (PPR) (mod. Black v4, Formlabs) and a layer resolution of 50 μm . Its morphology was chosen in accordance with the type IV specimen, reported in the ASTM D638-14 standard. Such a standard is designed to reproduce tensile property data for the evaluation of plastic materials.

To allow the self-sensing feature, a FBG sensor (mod. SMF-28, Technica SA) was embedded into the sample. Geometrically, it had a diameter of about 242 μm , of which $(8.2 \pm 0.1) \mu\text{m}$ of core, $(125.0 \pm 0.7) \mu\text{m}$ of cladding and $(242 \pm 5) \mu\text{m}$ of an acrylate coating, and a length of the grating of 14 mm. While, optically, it presented a nominal wavelength of $(1559.98 \pm 0.05) \text{ nm}$ in transmission and reflection, a full-width at half maximum (FWHM) of 0.26 nm, a reflective bandwidth (RBW) @-3 dB of 0.26 nm and a reflectivity of 85.65 %. Specifically, the printing stage was interrupted when the central layer of the test sample was reached and the FBG sensor was carefully placed along the longitudinal axis of the same sample. Furthermore, some supports were also printed for pre-tensioning the FBG sensor and ensuring its correct blocking. Once this step was ended, the printing was restarted by completing the structure. At the end of the whole process, the printing supports were removed, and the test sample was first washed in isopropyl alcohol for 20 min and then cured under UV for 30 min (15 min for each side) at 60 $^{\circ}\text{C}$.

Together with the test sample, two additional compensation samples (compensation sample A and B), nominally identical to the previous one, were printed (Figure 1). A second FBG sensor (mod. SMF-28, Technica SA, nominal wavelength of $(1556.31 \pm 0.05) \text{ nm}$), encapsulated into a needle [27], and a K-type thermocouple were respectively embedded, adopting the same procedures already described. Their function was to acquire the thermal trend during the manufacturing process, allowing the apparent strain to be assessed. Consequently, the choice of this specific FBG was mainly determined by the fact that it was already investigated in [27], although calibrated as a thermometer.

2.2. Experimental setup and measurement procedures

The optical signal from the two FBG sensors was acquired by a spectrum analyzer (mod. SI 720, Micron Optics) and an optical interrogator (mod. DI 410, HBM), characterized by accuracies of $\pm 3 \text{ pm}$ and of $\pm 1 \text{ pm}$, respectively. Instead, a specific data acquisition system (DAQ, mod. USB-TEMP, Measurement Computing) was used to record the output voltage from the thermocouple.

After the curing stage, the test sample was left to rest for 30 min at room temperature, to guarantee its thermal stabilization, and subjected to a tensile stress by means of a testing machine (mod. ElectroPlus E3000, Instron). A load cell of $\pm 5 \text{ kN}$ and an

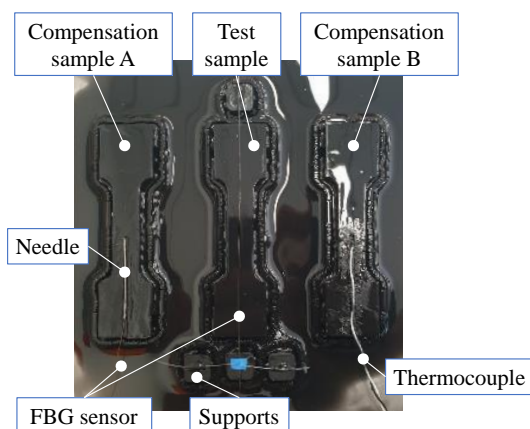


Figure 1. Details of the samples during the SLA printing process.

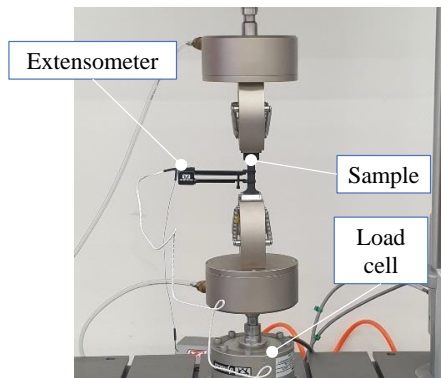


Figure 2. Details of the validation tests.

Table 1. Testing parameters.

Parameter (Unit)	Value
Sampling frequency of testing machine (Hz)	10
Preload (N)	10
Loading speed (mm/min)	1
Sampling frequency of optical interrogator (Hz)	10
Sampling frequency of spectrum analyser (Hz)	100
Sampling frequency of temperature DAQ (Hz)	10

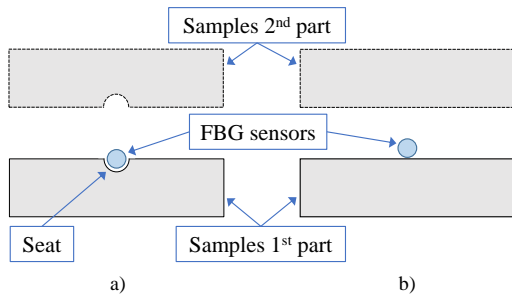


Figure 3. Scheme of configuration a) with seat and b) without seat. Images not in scale.

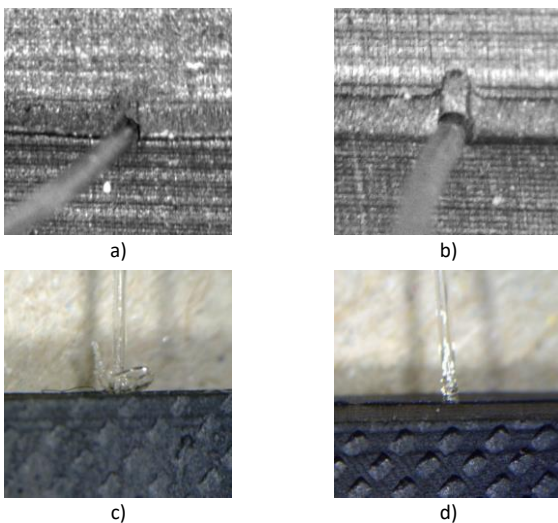


Figure 4. Typical microscope images of two representative specimens of the configuration with seat (a and c) and without seat (b and d) before and after the tensile test, respectively.

extensometer (mod. extensometer 12.5 mm class B-2, Instron) were used to measure the applied force and the consequent strain, respectively (Figure 2).

The testing parameters, in accordance with ASTM D638-14, are shown in Table 1.

3. PRELIMINARY ANALYSIS

Preliminary tests were carried out to evaluate the aspects related to the embedding process of the FBG sensor into the test sample.

3.1. Embedding process of the sensor in the self-sensing structure

At the beginning, three compact specimens, i. e. without the FBG sensor, were printed and subjected to a tensile test to determine their mechanical characteristics. Then the elastic modulus, equal to about (3.53 ± 0.09) GPa, and the elastic range, up to 300 N were measured.

After that, two different ways of embedding the FBG sensor into the test sample were investigated (Figure 3). In the first one (configuration with seat) an optical fiber, without Bragg grating and with same dimensions as the FBG sensor, was placed and pre-tensioned in a circular seat. Such a seat, having a radius of $150 \mu\text{m}$, was provided on the longitudinal axis of the test sample in correspondence of its central layer. Instead, in the second one (configuration without seat), the optical fiber was simply laid and pre-tensioned in the middle of the central layer. Hence, further six specimens, three for each configuration, were tested. These strategies are different to those reported in the literature for SLA. In [26], the main drawback that can be found is the difficulty of guaranteeing optimal incorporation of the FBG sensor. In fact, if the thickness and the width of the printed structure is high, there is a significant risk of obtaining an incomplete polymerization process and therefore the imperfect transfer of the load to the FBG sensor itself.

3.2. Mechanical characteristics of the embedding process

The configuration with seat (Figure 4 a) highlighted a lack of continuity, caused by the interruption of the printing to allow the positioning of the optical fiber. After the tensile test (Figure 4 c), the optical fiber undergoes a marked dismemberment of its cladding as proof of a good embedding into the printing material. On the other hand, the configuration without seat (Figure 4 b), in addition to presenting the same lack of continuity for the reasons already described, generates a relevant distortion of the upper layers of the specimen. Finally, at failure (Figure 4 d), the strain in the optical fiber suggests a lower adherence with the printing material than in the previous case.

Figure 5 describes the force-displacement curves, obtained from the tensile test, relating to the compact specimens with seat and without seat. The presence of the optical fiber inside the specimens leads to a slight weakening of the self-sensing structures in terms of load and elongation at failure. Generally, it is probably attributable to a higher speed of propagation of the crack, in turn due to the introduction of a discontinuity (optical fiber) into the material. Quantitative data are reported in Table 2. Specifically, the configuration with seat presents a lower reduction of fracture load (4.4 %) than the configuration without seat (7.1 %). That is caused, in an indiscernible way, by the polymerization of the PPR inside the seat and by the distortion of the layers above the optical fiber. However, in the elastic range, all the specimens have a rather limited variation of the elastic modulus (-1.6 % for specimens with seat and -3.5 % without seat referred to the average maximum stress in the elastic

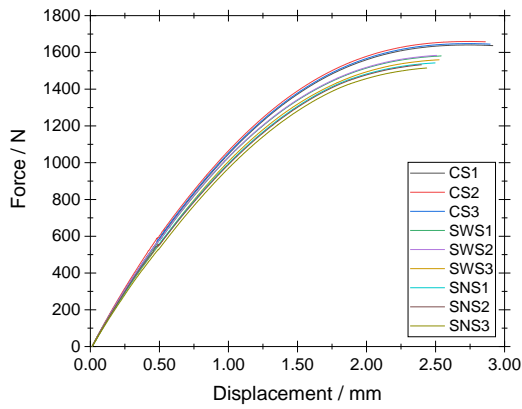


Figure 5. Force-displacement curves for the compact specimens (CS) with seat (SWS) and without seat (SNS).

Table 2. Results of tensile test for different type of specimens.

Type of specimen	Average fracture load in N	Standard deviation in N	Reduction* of fracture load in N
Compact specimens	1647	11	-
Specimens with seat	1574	13	4.4
Specimens without seat	1530	14	7.1

* referred to the average fracture load of the compact specimens.

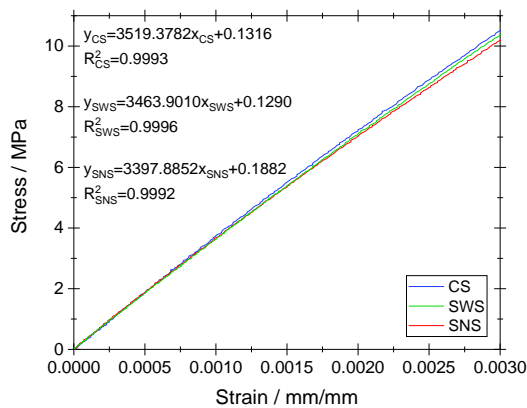


Figure 6. Average trends of the stress-strain curves in elastic range for compact specimens (CS) with seat (SWS) and without seat (SNS).

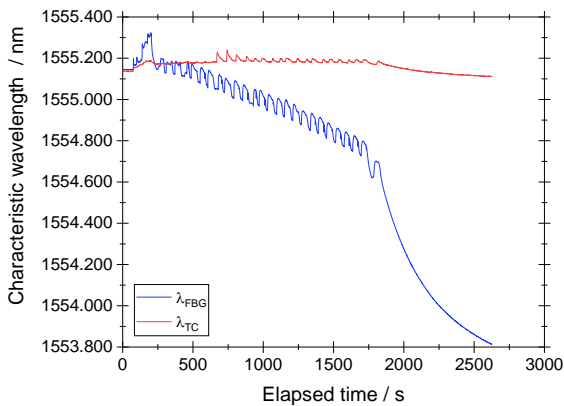


Figure 7. Time history of the characteristic wavelength of the FBG sensors embedded into the test sample (λ_{FBG}) and into the compensation sample A (λ_{TC}) during the printing stage.

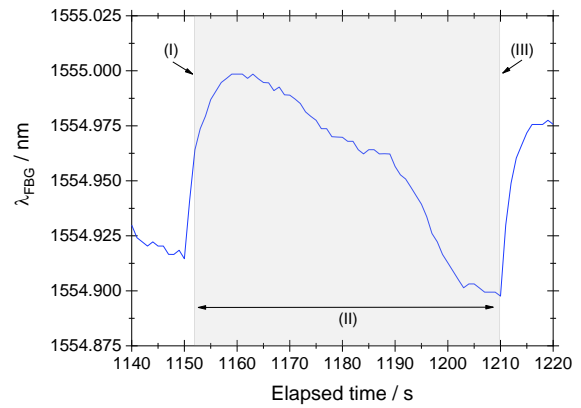


Figure 8. Detail of the time history of the characteristic wavelength of the FBG sensor embedded into the test sample (λ_{FBG}) during the printing stage - (I) = start immersion of the build platform in the PPR, (II) = generation of the single layer and (III) = start of emersion of the build platform from the PPR.

range of the compact specimens). For this reason, in terms of self-sensing, the different configurations are sufficiently superimposable (Figure 6).

Taking into account the performed preliminary analysis, and considering that the seat also acts as a visual guide during the placing and pre-tensioning phases of the FBG sensor, the choice of the most suitable configuration fell on the one with seat.

4. RESULTS

In this section, results concerning the monitoring of the 3D printing process and the mechanical behaviour (elastic stage) of the self-sensing assembled structure, are reported.

4.1. Monitoring of the stereolithographic printing process

Figure 7 displays the trends of the characteristic wavelength of the FBG sensors embedded into the test sample and into the compensation sample A as a function of elapsed time during the printing stage. Locally, both curves are characterized by a cyclic trend due to the movement of the build platform, i.e., its immersion in the PPR bath, the generation of the single layer and its emersion (Figure 8). However, as expected, the FBG sensor embedded into the compensation sample A is less affected by this condition. In fact, its encapsulation inside a needle considerably reduces the strain to which it is subject, favoring the measurement of the apparent strain caused by the variation of the temperature. Generally, the FBG sensor into the test sample exhibits a reduction in the pitch of the Bragg grating, attributable to a state of compression induced by the polymerization of the PPR.

Figure 9 compares the trends of the characteristic wavelength of the FBG sensor into the compensation sample A and of the thermocouple into the compensation sample B during the printing stage. In this case, the two signals present a good coherence up to 700 s from to the printing re-start, i.e. from the printing start of the second half of the sample. After that, a visible divergence occurs probably because of a localized strain of the needle due to the excessive heating of the layers above the center line and the consequent state of compression, induced by the polymerization of the PPR.

In conclusion, the signal of the FBG sensor into the test sample was suitably compensated by that of the apparent strain recorded by the second FBG into the compensation sample A. Figure 10 presents the compensated signal along the whole

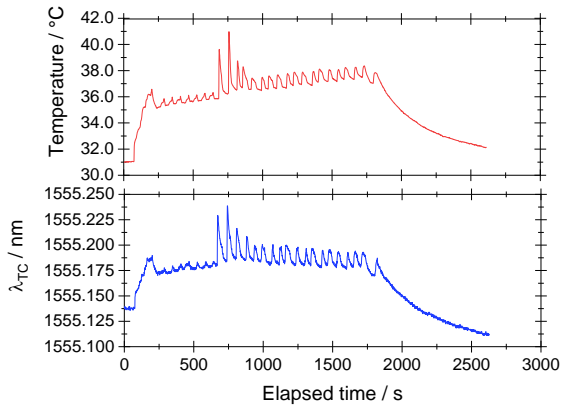


Figure 9. Time history of the characteristic wavelength of the FBG sensor embedded into the compensation sample A (λ_{TC}) and of the temperature measured by the thermocouple into the compensation sample B during the printing stage.

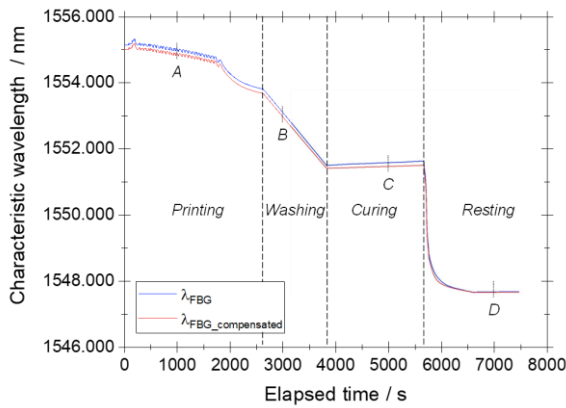


Figure 10. Time history of the characteristic wavelengths of the FBG sensor embedded into the test sample before (λ_{FBG}) and after compensation ($\lambda_{FBG_compensated}$) during the whole manufacturing process.

Table 3. Characteristic wavelengths of the FBG sensor embedded into the test sample before (λ_{FBG}) and after compensation ($\lambda_{FBG_compensated}$).

Point	Elapsed time in s	λ_{FBG} in nm	$\lambda_{FBG_compensated}$ in nm	$\Delta\lambda^*$ in nm
A	1000	1555.020	1554.853	0.167
B	3000	1553.098	1552.938	0.159
C	5000	1551.578	1551.484	0.094
D	7000	1547.718	1547.709	0.009

*computed as $\Delta\lambda = \lambda_{FBG} - \lambda_{FBG_compensated}$

manufacturing process of the self-sensing structure. The major differences between the raw signal (λ_{FBG}) and the compensated one ($\lambda_{FBG_compensated}$) are visible in the printing and curing stages. Instead, in the washing and resting stages the curves are sufficiently superimposable after an initial transient. Furthermore, all stages, except for the curing one, are subject to a reduction in the characteristic wavelength and therefore to a consequent state of compression. Globally, these trends are attributable to the effects of the polymerization of the single layers (compression) and the hardening of the structure of the structure (relaxation).

Table 3 shows the values of the characteristic wavelengths of the FBG sensor into the test sample at specific time (Figure 10).

Conservatively, the uncertainty of the characteristic wavelength of the FBG sensor embedded into the test sample

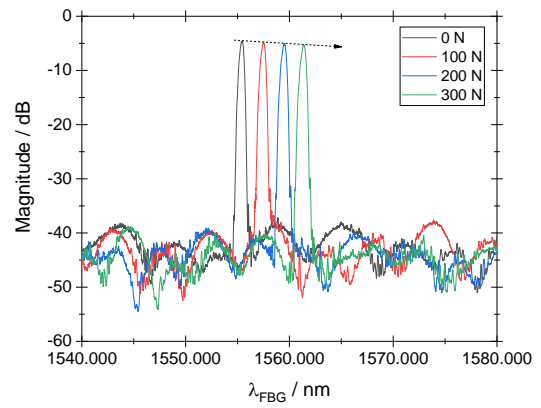


Figure 11. Variation of the magnitude of the optical signal of FBG sensor as a function of the wavelength at a load application on the test sample.

Table 4. Results of tensile tests for different type of specimens.

Load in N	Peak wavelength in nm	Peak magnitude in dB	Standard deviation in dB
0	1555.428	-4.62	0.05
100	1557.516	-4.86	0.05
200	1559.504	-5.06	0.05
300	1561.368	-5.27	0.05

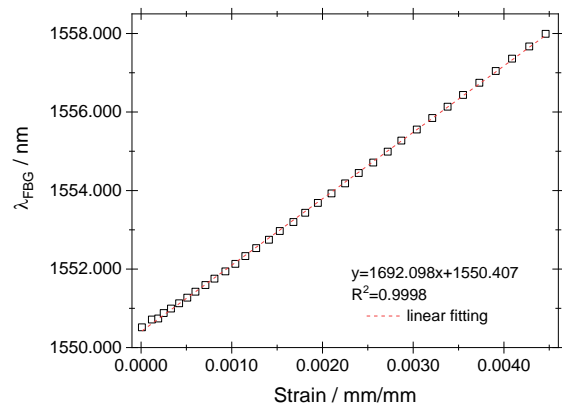


Figure 12. Calibration curve of the FBG sensor used to measure the tensile strain on the test sample.

(λ_{FBG}) was estimated as type B [28], based on the accuracy of the spectrum analyzer used for these measurements. Therefore, a uniform distribution (i.e. rectangular) with an amplitude of ± 0.003 nm was considered from which a value of type B uncertainty equal to about ± 0.0017 nm was estimated.

4.2. Mechanical performance of the self-sensing structure

Figure 11 exhibits the spectrum of the FBG sensor as the load on the test sample varies, however remaining in elastic range. The tensile phase induces a shift of the peak to greater wavelengths and a reduction of the magnitude of the optical signal due to the increase of the pitch of the Bragg grating (Table 4). In this case the uncertainty was estimated as type A [28] on the magnitude of the optical signal at 300 N with a value of about 0.01 dB.

Finally, Figure 12 reports the calibration curve relating to the tensile strain measured by the test sample. As well-known from the literature [29] and as can be seen also from Figure 11, the plotted curve has a good linearity.

5. CONCLUSIONS

The paper discusses the development of self-sensing structures printed in SLA and equipped with a FBG sensor.

The presented study allows to state that a FBG sensor can be suitably embedded into a structure printed in SLA. This integration is optimal when a seat is created, since it guarantees the advantageous placing of the FBG sensor and the determination of a good interface for the transfer of the load without making use of further post-production methods. In addition, such a work shows how a FBG sensor can monitor the stress state induced into a structure throughout its printing process (i.e., printing, washing and curing stages). To obtain this, the use of compensation strategies, implemented through appropriate compensation sensors embedded in similar structures and subjected to the same process, is decisive. This represents an innovative approach of investigation as it allows obtaining information directly related to the printed product without resorting to more complex and often difficult to apply investigations during the printing itself. Finally, the self-sensing structure shows an appropriate structural response when subjected to a controlled stress.

The main limitation of the proposed work relates to the fact that, because of the movement of the build platform of the SLA printer, the FBG sensor could be erroneously embedded into the structure and consequently the quantity of interest could not be correctly measured. Such an issue is addressed here by adopting some supports for pre-tensioning the FBG sensor, capable of ensuring its correct blocking. However, this procedure cannot always be easily ensured, especially when the self-sensing structure has a complex geometry. Furthermore, the same FBG sensor could require a tortuous positioning such as to disperse the light beam inside it, making the measurement impossible, or to produce its breakage, being constituted by a glass fiber.

Future developments will be focused on the study of the thermo-mechanical effect due to the printing process variables on the self-sensing structure and on the monitoring of a complex and functional self-sensing structure, equipped with a multi-sensor FBG system.

REFERENCES

- [1] E. Mesquita, P. Antunes, F. Coelho, P. André, A. Arêde, H. Varum, Global overview on advances in structural health monitoring platforms, *Journal of Civil Structural Health Monitoring* 6 (2016), pp. 461-47, DOI: [10.1007/s13349-016-0184-5](https://doi.org/10.1007/s13349-016-0184-5)
- [2] H. Rocha, C. Semprinoschnig, J. P. Nunes, Sensors for process and structural health monitoring of aerospace composites: A review, *Engineering Structures* 237 (2021) n. 112231, DOI: [10.1016/j.engstruct.2021.112231](https://doi.org/10.1016/j.engstruct.2021.112231)
- [3] E. Mesquita, A. Arêde, R. Silva, P. Rocha, A. Gomes, N. Pinto, P. Antunes, H. Varum, Structural health monitoring of the retrofitting process, characterization and reliability analysis of a masonry heritage construction, *Journal of Civil Structural Health Monitoring* 7 (2017), pp. 405-428, DOI: [10.1007/s13349-017-0232-9](https://doi.org/10.1007/s13349-017-0232-9)
- [4] Z. Gao, X. Zhu, Y. Fang, H. Zhang, Active monitoring and vibration control of smart structure aircraft based on FBG sensors and PZT actuators, *Aerospace Science and Technology* 63 (2017), pp. 101-109, DOI: [10.1016/j.ast.2016.12.027](https://doi.org/10.1016/j.ast.2016.12.027)
- [5] A. Quattrocchi, R. Montanini, M. Latino, N. Donato, Development and characterization of a fiber Bragg grating ethanol sensor for liquids, *Proc. of the 22nd International Workshop on ADC and DAC Modelling and Testing*, Palermo, Italy, 14-16 September 2020, pp. 55-59. Online [Accessed 11 April 2023] <https://www.imeko.org/publications/tc4-2020/IMEKO-TC4-2020-11.pdf>
- [6] A. Quattrocchi, R. Montanini, M. Latino, N. Donato, PMMA-coated fiber Bragg grating sensor for measurement of Ethanol in liquid solution: manufacturing and metrological evaluation, *Acta IMEKO* 10(2) (2021), pp. 133-138, DOI: [10.21014/acta_imeko.v10i2.1052](https://doi.org/10.21014/acta_imeko.v10i2.1052)
- [7] Z. Ma, X. Chen, Fiber Bragg gratings sensors for aircraft wing shape measurement: Recent applications and technical analysis, *Sensors* 19 (2018), art. no. 55, DOI: [10.3390/s19010055](https://doi.org/10.3390/s19010055)
- [8] T. H. Loutas, P. Charlftis, A. Airoidi, P. Bettini, C. Koimtzoglou, V. Kostopoulos, Reliability of strain monitoring of composite structures via the use of optical fiber ribbon tapes for structural health monitoring purpose, *Compos. Struct.* 134 (2015), pp. 762-771, DOI: [10.1016/j.compstruct.2015.08.100](https://doi.org/10.1016/j.compstruct.2015.08.100)
- [9] A. Montero, I. S. de Ocariz, I. Lopez, P. Venegas, J. Gomez, J. Zubia, Fiber Bragg Gratings, IT techniques and strain gauge validation for strain calculation on aged metal specimens, *Sensors* 11 (2011), pp. 1088-1104, DOI: [10.3390/s110101088](https://doi.org/10.3390/s110101088)
- [10] L. F. Ferreira, P. Antunes, F. Domingues, P. A. Silva, P. S. André, Monitoring of sea bed level changes in nearshore regions using fiber optic sensors, *Measurement* 45 (2012), pp. 1527-1533, DOI: [10.1016/j.measurement.2012.02.026](https://doi.org/10.1016/j.measurement.2012.02.026)
- [11] J. Leng, A. Asundi, Structural health monitoring of smart composite materials by using EFPI and FBG sensors, *Sensors Actuators A* 103 (2003), pp. 330-40, DOI: [10.1016/S0924-4247\(02\)00429-6](https://doi.org/10.1016/S0924-4247(02)00429-6)
- [12] U. M. N. Jayawickrema, H. M. C. M. Herath, N. K. Hettiarachchi, H. P. Sooriyaarachchi, J. A. Epaarachchi, Fibre-optic sensor and deep learning-based structural health monitoring systems for civil structures: a review, *Measurement* 199 (2022) art no. 111543, DOI: [10.1016/j.measurement.2022.111543](https://doi.org/10.1016/j.measurement.2022.111543)
- [13] M. Malekzadeh, M. Gul, F. N. Catbas, Use of FBG sensors to detect damage from large amount of dynamic measurements, *Topics on the Dynamics of Civil Structures*, Volume 1, pp. 273-281, Springer, New York, USA 2012, DOI: [10.1007/978-1-4614-2413-0_27](https://doi.org/10.1007/978-1-4614-2413-0_27)
- [14] L. Ren, Z.-G. Jia, H.-N. Li, G. Song, Design and experimental study on FBG hoop-strain sensor in pipeline monitoring, *Opt. Fiber Technol.* 20 (2014), pp. 15-23, DOI: [10.1016/j.yofte.2013.11.004](https://doi.org/10.1016/j.yofte.2013.11.004)
- [15] G. Allevi, L. Capponi, P. Castellini, P. Chiariotti, F. Docchio, F. Freni, R. Marsili, M. Martarelli, R. Montanini, S. Pasinetti, A. Quattrocchi, R. Rossetti, G. Rossi, G. Sansoni, E. P. Tomasini, Investigating additive manufactured lattice structures: a multi-instrument approach, *IEEE Transactions on Instrumentation and Measurement*, 69 (2019), pp. 2459-2467, DOI: [10.1109/TIM.2019.2959293](https://doi.org/10.1109/TIM.2019.2959293)
- [16] A. Quattrocchi, D. Alizzio, L. Capponi, T. Tocci, R. Marsili, G. Rossi, S. Pasinetti, P. Chiariotti, A. Annessi, P. Castellini, M. Martarelli, F. Freni, A. Di Giacomo, R. Montanini, Measurement of the structural behaviour of a 3D airless wheel prototype by means of optical non-contact techniques, *ACTA IMEKO* 11(3) (2022), pp. 1-8, DOI: [10.21014/acta_imeko.v11i3.1268](https://doi.org/10.21014/acta_imeko.v11i3.1268)
- [17] M. G. Zobel, K. Sugden, D. J. Webb, D. Sáez-Rodríguez, K. Nielsen, O. Bang, Embedding silica and polymer fibre Bragg gratings (FBG) in plastic 3D-printed sensing patches, *Microstructured and Specialty Optical Fibres IV* 9886 (2016), pp. 78-89, DOI: [10.1117/12.2228753](https://doi.org/10.1117/12.2228753)
- [18] R. Lima, R. Tavares, S. O. Silva, P. Abreu, M. T. Restivo, O. Frazão, Fiber Bragg grating sensor based on cantilever structure embedded in polymer 3D printed material. *Proc. of the 25th Optical Fiber Sensors Conference (OFS)*, Jeju, South Korea, 24-28 April 2017, pp. 1-4, DOI: [10.1117/12.2264600](https://doi.org/10.1117/12.2264600)

- [19] P. Lesiak, K. Pogorzelec, A. Bochenek, P. Sobotka, K. Bednarska, A. Anuszkiewicz, T. Osuch, M. Sienkiewicz, P. Marek, M. Nawotka, T. R. Woliński, Three-dimensional-printed mechanical Transmission Element with a Fiber Bragg Grating Sensor embedded in a replaceable measuring head, *Sensors* 22 (2022) art. no. 3381. DOI: [10.3390/s22093381](https://doi.org/10.3390/s22093381)
- [20] Y. F. Zhang, C. Y. Hong, R. Ahmed, Z. Ahmed, A fiber Bragg grating based sensing platform fabricated by fused deposition modeling process for plantar pressure measurement, *Measurement* 112 (2017), pp. 74-79. DOI: [10.1016/j.measurement.2017.08.024](https://doi.org/10.1016/j.measurement.2017.08.024)
- [21] L. Fang, T. Chen, R. Li, S. Liu, Application of embedded fiber Bragg grating (FBG) sensors in monitoring health to 3D printing structures, *IEEE Sensors Journal* 16 (2016), pp. 6604-6610. DOI: [10.1109/JSEN.2016.2584141](https://doi.org/10.1109/JSEN.2016.2584141)
- [22] Y. K. Lin, T. S. Hsieh, L. Tsai, S. H. Wang, C. C. Chiang, Using three-dimensional printing technology to produce a novel optical fiber Bragg grating pressure sensor, *Sensors Mater* 28(5) (2016), pp. 389-394. DOI: [10.18494/SAM.2016.1189](https://doi.org/10.18494/SAM.2016.1189)
- [23] C. Hong, Y. Yuan, Y. Yang, Y. Zhang, Z. A. Abro, A simple FBG pressure sensor fabricated using fused deposition modelling process, *Sensors and Actuators A: Physical* 285 (2019), pp. 269-274. DOI: [10.1016/j.sna.2018.11.024](https://doi.org/10.1016/j.sna.2018.11.024)
- [24] Z. A. Abro, C. Hong, Y. Zhang, M. Q. Siddiqui, A. M. R. Abbasi, Z. Abro, S. Q. B. Tariq, Development of FBG pressure sensors using FDM technique for monitoring sleeping postures, *Sensors and Actuators A: Physical* 331 (2021) art. no. 112921. DOI: [10.1016/j.sna.2021.112921](https://doi.org/10.1016/j.sna.2021.112921)
- [25] R. Montanini, G. Rossi, A. Quattrocchi, D. Alizzio, L. Capponi, R. Marsili, A. Di Giacomo, T. Tocci, Structural characterization of complex lattice parts by means of optical non-contact measurements. Proc. of the 2020 IEEE International Instrumentation and Measurement Technology Conference (I2MTC), Dubrovnik, Croatia, 25-28 May 2020, pp. 1-6. DOI: [10.1109/I2MTC43012.2020.9128771](https://doi.org/10.1109/I2MTC43012.2020.9128771)
- [26] N. R. Manzo, G. T. Callado, C. M. Cordeiro, L. C. M. Vieira, Embedding optical Fiber Bragg Grating (FBG) sensors in 3D printed casings, *Optical Fiber Technology* 53 (2019) art. no. 102015. DOI: [10.1016/j.yofte.2019.102015](https://doi.org/10.1016/j.yofte.2019.102015)
- [27] R. Montanini, L. D'Acquisto, Simultaneous measurement of temperature and strain in glass fiber/epoxy composites by embedded fiber optic sensors: I. Cure monitoring, *Smart Materials and Structures* 16 (2007), pp. 1718-1726. DOI: [10.1088/0964-1726/16/5/026](https://doi.org/10.1088/0964-1726/16/5/026)
- [28] Uncertainty of Measurement—Part 3: Guide to the Expression of Uncertainty in Measurement, document ISO/IEC Guide 98-3:2008, 2008
- [29] W. Shen, R. Yan, L. Xu, G. Tang, X. Chen, Application study on FBG sensor applied to hull structural health monitoring, *Optik*, 126 (2015), pp. 1499-1504. DOI: [10.1016/j.ijleo.2015.04.046](https://doi.org/10.1016/j.ijleo.2015.04.046)